universe

MDPI

Article

Molecular Gas Heating, Star Formation Rate Relations, and AGN Feedback in Infrared-Luminous Galaxy Mergers

Duncan Farrah [1,2,*], Andreas Efstathiou [3], Jose Afonso [4,5], David L. Clements [6], Kevin Croker [1], Evanthia Hatziminaoglou [7], Maya Joyce [8], Vianney Lebouteiller [9], Aláine Lee [2], Carol Lonsdale [10], Chris Pearson [11,12,13], Sara Petty [14,15], Lura K. Pitchford [16,17], Dimitra Rigopoulou [13], Aprajita Verma [13] and Lingyu Wang [18,19]

1 Department of Physics and Astronomy, University of Hawai'i, 2505 Correa Road, Honolulu, HI 96822, USA
2 Institute for Astronomy, 2680 Woodlawn Drive, University of Hawai'i, Honolulu, HI 96822, USA
3 School of Sciences, European University Cyprus, Diogenes Street, Engomi, 1516 Nicosia, Cyprus
4 Instituto de Astrofísica e Ciências do Espaço, Universidade de Lisboa, 1349-018 Lisboa, Portugal
5 Departamento de Física, Faculdade de Ciências, Universidade de Lisboa, 1749-016 Lisboa, Portugal
6 Blackett Laboratory, Imperial College London, Prince Consort Road, London SW7 2AZ, UK
7 European Southern Observatory, Karl-Schwarzschild-Str 2, D-85748 Garching bei München, Germany
8 Department of Physics and Astronomy, Michigan State University, East Lansing, MI 48824, USA
9 Laboratoire AIM, Université Paris-Saclay, 91191 Gif-sur-Yvette, France
10 National Radio Astronomy Observatory, 520 Edgemont Road, Charlottesville, VA 22903, USA
11 RAL Space, STFC Rutherford Appleton Laboratory, Didcot OX11 0QX, UK
12 School of Physical Sciences, The Open University, Milton Keynes MK7 6AA, UK
13 Oxford Astrophysics, University of Oxford, Keble Rd, Oxford OX1 3RH, UK
14 NorthWest Research Associates, 3380 Mitchell Ln., Boulder, CO 80301, USA
15 Convent & Stuart Hall Schools of the Sacred Heart, 2222 Broadway, San Francisco, CA 94115, USA
16 George P. and Cynthia Woods Mitchell Institute for Fundamental Physics and Astronomy, Texas A&M University, College Station, TX 77845, USA
17 Department of Physics and Astronomy, Texas A&M University, College Station, TX 77843, USA
18 SRON Netherlands Institute for Space Research, Landleven 12, 9747 AD Groningen, The Netherlands
19 Kapteyn Astronomical Institute, University of Groningen, Postbus 800, 9700 AV Groningen, The Netherlands
* Correspondence: dfarrah@hawaii.edu

Citation: Farrah, D.; Efstathiou, A.; Afonso, J.; Clements, D.L.; Croker, K.; Hatziminaoglou, E.; Joyce, M.; Lebouteiller, V.; Lee, A.; Lonsdale, C.; et al. Molecular Gas Heating, Star Formation Rate Relations, and AGN Feedback in Infrared-Luminous Galaxy Mergers. *Universe* **2023**, *9*, 3. https://doi.org/10.3390/universe9010003

Received: 29 August 2022
Revised: 29 October 2022
Accepted: 16 December 2022
Published: 21 December 2022

Abstract: We examine the origin of molecular gas heating in a sample of 42 infrared-luminous galaxies at $z < 0.3$ by combining two sets of archival data: first, integrated CO line luminosities in the 1–0 and 5–4 through 13–12 transitions; second, results from radiative transfer modelling that decompose their bolometric emission into starburst, AGN, and host galaxy components. We find that the CO 1–0 and 5–4 through 9–8 lines primarily arise via radiative heating in the starburst and the host galaxy. In contrast, the CO 10–9 through 13–12 lines may arise primarily in the starburst and AGN, with an increasing contribution from mechanical heating and shocks. For the sample as a whole, we find no evidence that AGN luminosity affects the heating of molecular gas by star formation. However, for starbursts with low initial optical depths, a more luminous AGN may reduce the efficiency of starburst heating of the CO 5–4 and above lines, consistent with negative AGN feedback.

Keywords: galaxy formation; galaxy evolution; infrared-luminous galaxy; starburst galaxy

1. Introduction

A fundamental channel for galaxy assembly at $z \gtrsim 1$ is the conversion of molecular gas to stellar and supermassive black hole (SMBH) mass in brief ($\sim 10^8$ yr) but intense episodes of activity. These episodes, which are almost invariably heavily obscured and thus most luminous at infrared wavelengths, can harbor star formation rates (SFRs) of up to several thousand Solar masses per year [1], and can increase SMBH masses by up to $\sim$1 dex [2]. At low redshifts, infrared-luminous galaxies are rare, but are almost invariably observed to be mergers [3–9] and usually harbor both intense starbursts and luminous AGN [10–18]. Some

fraction of local infrared-luminous galaxies later go through an optical QSO phase [19–21]. Studies of infrared-luminous galaxies at low-redshift are invaluable for understanding the physics of obscured star formation and AGN, and as a zeropoint for studying the redshift evolution of this population. Infared-luminous galaxies at high redshift may have a lower merger fraction [22–26] but can also harbor higher SFRs and more luminous AGN [1,27–42]. Reviews of the infrared-luminous phases of galaxy assembly and extragalactic infrared astronomy can be found in [43–49].

The heating of molecular gas in infrared-luminous galaxies is thus an important diagnostic of both the conversion of molecular gas to stellar and SMBH mass, and of the impact of starburst and AGN activity on the interstellar medium (ISM) of their host galaxies [50–54]. While the bulk of the molecular gas in galaxies is in the form of 'cold' H_2, this molecule's lack of a dipole means that cold H_2 is challenging to observe directly[1]. Instead, the molecular gas is usually traced via observations of rotational transitions of carbon monoxide (^{12}CO, CO hereafter), since CO has both a strong dipole moment and relatively low-lying energy transitions. The ground state transition (J = 1–0) and transitions up to about J = 4–3 of CO are good tracers of the total molecular gas reservoir in galaxies [56–63]. The higher J transitions trace the warmer, denser molecular gas associated with starbursts and AGN (e.g., [64–68]). As a result, observations of CO emission in high-redshift galaxies have produced important insights into galaxy assembly processes [39,69,70].

Significant uncertainties remain over how different transitions of CO are produced. In principle, CO emission can arise in star-forming regions, AGN, or in the ISM heated by passively evolving stellar populations; One way to address this is to model physical conditions in the line-emitting gas using multiple transitions of CO simultaneously [71,72]. Another approach is to compare CO line luminosities to the total infrared luminosity of the galaxy [65]. However, ambiguities in the power source behind the infrared emission persist in this approach.

In this paper, we take an alternative approach to determining the origin of CO heating in infrared-luminous galaxies. We take a sample of 42 gas-rich mergers with infrared luminosities in excess of 10^{12} $L_\odot$ at $z < 0.3$, for which we have completed radiative transfer modelling which constrains their starburst, AGN, and host galaxy luminosities. We then assemble archival observations of the 1–0 and 5–4 through 13–12 transitions of CO for this sample, and compare them to the component luminosities from the radiative transfer modelling to infer the origin of the CO gas heating as a function of rotational quantum number. Throughout, we assume $H_0 = 70\,\mathrm{km\,s^{-1}\,Mpc^{-1}}$, $\Omega = 1$, and $\Omega_\Lambda = 0.7$. We convert all literature data to this cosmology where necessary.

2. Methods

2.1. Sample Selection

The sample selection is described in full in [2,73], and is summarized here. The sample includes ultraluminous infrared galaxies (ULIRGs, systems with rest-frame 1–1000 μm luminosities in excess of 10^{12} $L_\odot$) with IRAS 60 μm fluxes greater than ∼2Jy that were assembled for the HERschel ULIRG Reference Survey [16,68,74,75]. This sample is representative of ULIRGs in the low-redshift Universe as it comprises nearly all known systems with $L_{IR} < 10^{12}$ $L_\odot$ at $z < 0.27$. The sample spans approximately one order of magnitude in total infrared luminosity, includes merger stages from early to late stage, and all four primary optical spectral classes (HII, LINER, Sy2, Sy1). The host galaxy properties are typical of massive, gas-rich galaxies in the local Universe. These data and diagnostic plots are given in [2,73].

2.2. Molecular Gas Data

We use the CO 1–0 transition, which traces cold molecular gas, and the CO 5–4 through 13–12 transitions, which trace hotter molecular gas. We explored the possibility of using the 2–1 through 4–3 lines, and in lines above 13–12. There are, however, insufficient observations of our sample in these lines to enable a statistical analysis. For CO 1–0 we use

the compilation presented in Farrah et al. [2]. These data are mostly taken from Kamenetzky et al. [76], and/or a wider set of archival observations [56,67,77–94]. For the 5–4 through 13–12 lines, we assemble data from Pearson et al. [68], who present a homogeneous analysis of these lines as observed by the SPIRE instrument onboard *Herschel*. Data for a few objects are also taken from Kamenetzky et al. [76]. In all cases, the CO line observations are spatially unresolved. Spatially resolved, interferometric observations of about a quarter of our sample exist, but we use spatially unresolved observations in all cases to give a consistent analysis.

2.3. Infrared Emission Data

We adopt the results from Efstathiou et al. [73]. This study decomposes the emission from our sample into contributions from a starburst, an AGN, and the host galaxy. The results from this study are consistent with previous SED modelling works, and provide derived physical parameters for each component. The complete set of parameters for each model, and their adopted ranges, are given in Table 2 of [73].

The starburst model [95] assumes an exponentially decaying burst of star formation. The model includes a range of possible initial optical depths of the star-forming clouds, e-folding times of the starburst, and a range in starburst ages, thus tracking multiple possible evolutionary paths for the molecular clouds hosting the star formation.

The AGN model [96–98] assumes a smooth, tapered disk in which the half-opening angle of the torus, the inclination angle of the torus relative to the observer, the ratio of inner to outer radius, and equatorial optical depth, can all vary. The AGN model also includes luminosities derived by integrating the observed emission over 4π steradians, as well as luminosities that include a correction for the anisotropic structure of the obscurer.

The host model assumes a Sérsic profile with $n = 4$. The stars and dust are mixed, rather than the extinction applied as a foreground screen. The three parameters of the host model are the e-folding time of the star formation, the optical depth of the host, and the intensity of starlight.

For our study, the key extracted physical quantities from the radiative transfer models are:

- L^o_{tot}: the total rest-frame infrared (1–1000 μm) luminosity, uncorrected for anisotropic AGN emission.
- L_{Sb}, $\dot{M}_{Sb}$: the rest-frame infrared luminosity of the starburst, and the SFR in the starburst averaged over the starbursts age, excluding the host.
- L_h, $\dot{M}_h$: the rest-frame infrared luminosity and SFR of the host galaxy, excluding the starburst.
- L^o_{AGN}, L^c_{AGN}: Observed and anisotropy-corrected rest-frame infrared luminosity of the AGN.
- τ_V: the initial optical depth of giant molecular clouds in the starburst, with an allowed range of $50 < \tau_V < 250$.

A description of these quantities is given in Efstathiou et al. [73].

3. Results and Discussion

3.1. Correlations with Total Infrared Luminosity

We first examine the relations between the CO luminosities and the total observed infrared luminosities (L^o_{tot}). Using the Kendall-τ test, we find significant correlations ($\tau > 0.38$, $p < 0.01$) between all CO line luminosities and L^o_{tot}. The p-values are plotted as the black line in Figure 1.

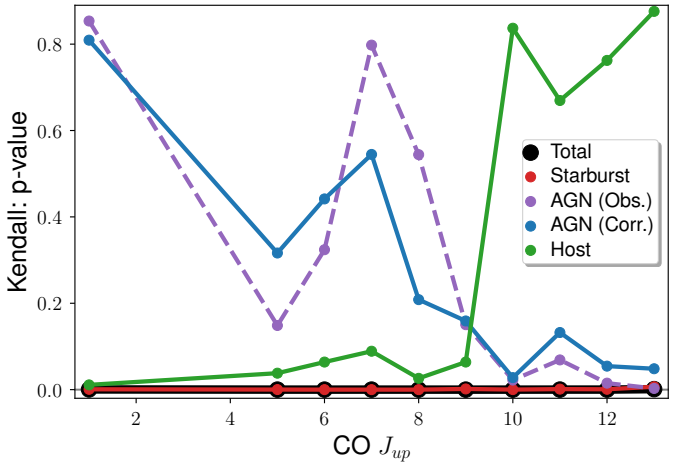

Figure 1. The p-values from the Kendall-τ tests, comparing the CO luminosities to the total, starburst, AGN, and host infrared luminosities (Sections 3.1 and 3.2). A low p-value indicates that the hypothesis of no correlation can be rejected.

We next derive relations between CO luminosity and L^{o}_{tot}, of the form:

$$\log(L_{CO}) = \mathcal{A}\log(L^{o}_{tot}) + \mathcal{B} \quad (1)$$

We used the Orthogonal Distance Regression algorithm [99] as implemented within the *SciPy* Python library using a random seed of 2001. This yields:

$$\log(L_{1\text{–}0}) = 0.78 \pm 0.17 \log(L^{o}_{Tot}) - 4.02 \pm 2.07 \quad (2)$$
$$\log(L_{5\text{–}4}) = 0.92 \pm 0.18 \log(L^{o}_{Tot}) - 3.78 \pm 2.17 \quad (3)$$
$$\log(L_{6\text{–}5}) = 1.14 \pm 0.23 \log(L^{o}_{Tot}) - 6.44 \pm 2.76 \quad (4)$$
$$\log(L_{7\text{–}6}) = 1.40 \pm 0.23 \log(L^{o}_{Tot}) - 9.65 \pm 2.79 \quad (5)$$
$$\log(L_{8\text{–}7}) = 1.30 \pm 0.25 \log(L^{o}_{Tot}) - 8.33 \pm 3.08 \quad (6)$$
$$\log(L_{9\text{–}8}) = 1.63 \pm 0.33 \log(L^{o}_{Tot}) - 12.38 \pm 3.99 \quad (7)$$
$$\log(L_{10\text{–}9}) = 1.39 \pm 0.27 \log(L^{o}_{Tot}) - 9.50 \pm 3.30 \quad (8)$$
$$\log(L_{11\text{–}10}) = 0.25 \pm 0.15 \log(L^{o}_{Tot}) + 4.31 \pm 1.86 \quad (9)$$
$$\log(L_{12\text{–}11}) = 0.04 \pm 0.15 \log(L^{o}_{Tot}) + 6.79 \pm 1.88 \quad (10)$$
$$\log(L_{13\text{–}12}) = 0.22 \pm 0.17 \log(L^{o}_{Tot}) + 4.56 \pm 2.01 \quad (11)$$

(see also, e.g., Greve et al. [65]). The slopes as a function of J_{up} are plotted in Figure 2. The slopes are consistent with a linear relation between L_{CO} and L^{o}_{tot} for J = 10–9 and below, but a sub-linear, possibly flat relation for J = 11–10 and above. Some example fits are presented in Figure 3.

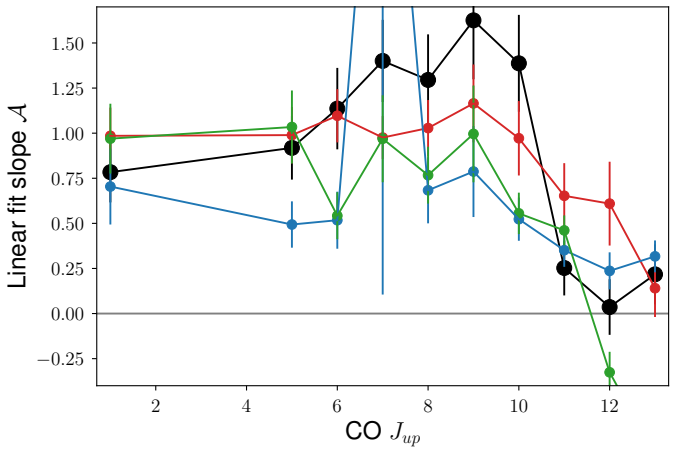

Figure 2. The slopes of the fits between CO luminosity and total, starburst, host, and AGN luminosity, using Equation (1) (Sections 3.1 and 3.2). The colors follow the Figure 1 legend.

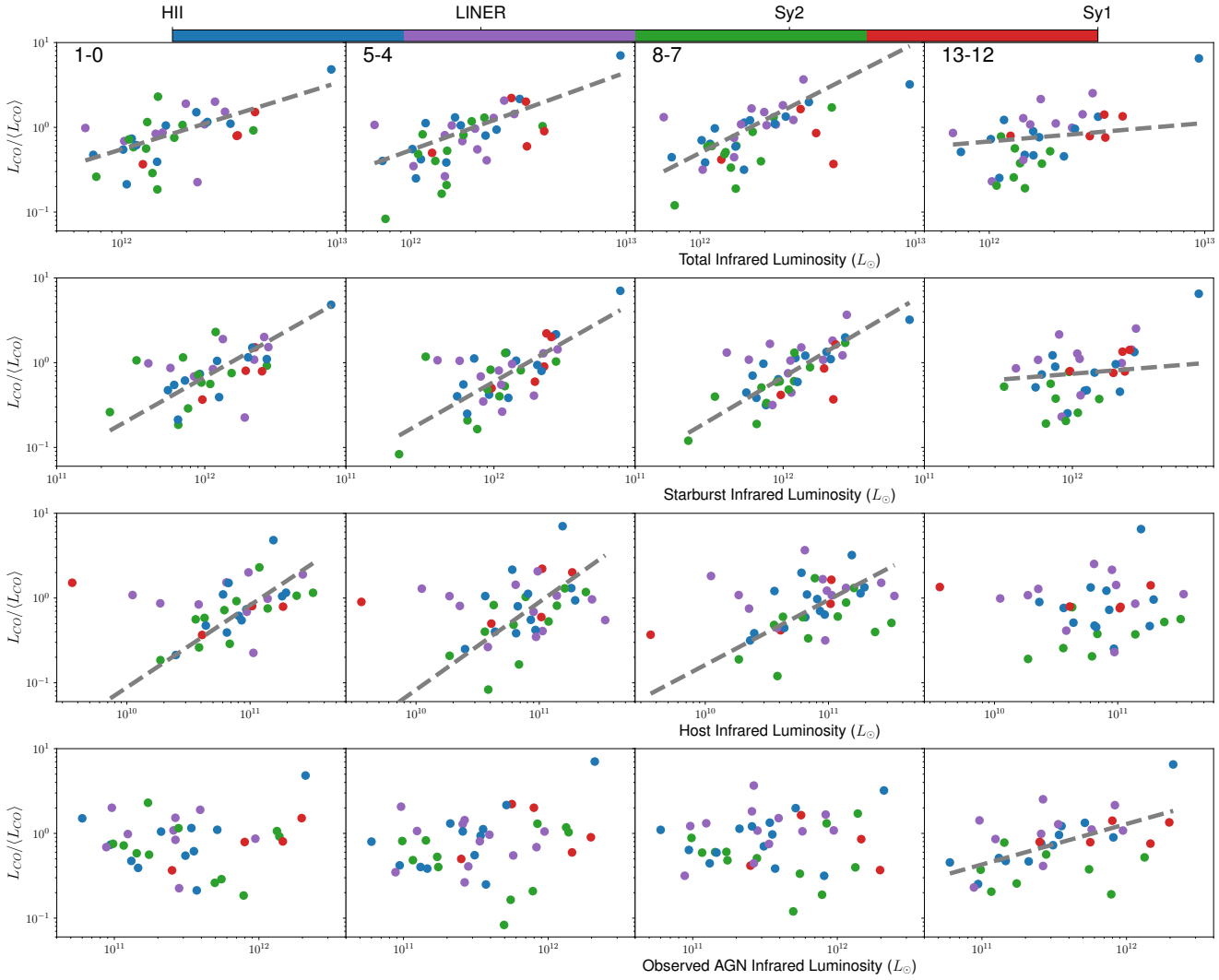

Figure 3. Example relations between CO line luminosities L_{CO} (Table 1), normalized by the relevant mean CO luminosity $\langle L_{CO}\rangle$, and total, starburst, host, and observed AGN infrared luminosities (Sections 3.1 and 3.2). The best-fit relations are plotted, if there is evidence for a correlation. No strong dependence on optical spectral type is observed.

Table 1. The sample and their CO luminosities. All luminosities are derived from measurements using single-aperture telescopes (Section 2.2). Units are 10^6 $L_\odot$. Uncertainties are 1σ.

Name	1–0	5–4	6–5	7–6	8–7	9–8	10–9	11–10	12–11	13–12
IRAS 00188-0856	0.10 ± 0.01	12.9 ± 10.8	9.3 ± 8.1	27.1 ± 10.1	35.4 ± 9.6	54.8 ± 9.6	39.1 ± 8.3	11.9 ± 9.2	41.1 ± 8.3	—
IRAS 00397-1312	2.12 ± 0.69	223.2 ± 44.1	138.3 ± 43.0	—	105.3 ± 43.0	114.1 ± 43.5	147.1 ± 43.5	—	181.9 ± 82.7	140.0 ± 44.1
IRAS 01003-2238	—	—	15.2 ± 9.7	10.5 ± 5.6	10.4 ± 7.8	62.2 ± 7.7	42.1 ± 16.2	33.1 ± 7.1	22.8 ± 7.1	19.3 ± 7.1
IRAS 03158+4227	0.40 ± 0.04	32.7 ± 11.8	58.7 ± 11.8	54.0 ± 12.0	56.2 ± 11.8	—	54.2 ± 11.4	36.3 ± 11.4	—	—
IRAS 03521+0028	0.48 ± 0.17	40.9 ± 29.4	67.2 ± 12.8	34.0 ± 16.3	59.7 ± 12.8	—	72.9 ± 14.2	46.6 ± 12.8	36.1 ± 12.8	21.3 ± 14.2
IRAS 05189-2524	0.13 ± 0.01	5.2 ± 1.0	7.1 ± 1.0	8.8 ± 1.1	11.0 ± 1.0	11.0 ± 0.9	14.0 ± 1.4	10.1 ± 0.9	8.4 ± 0.9	8.1 ± 0.9
IRAS 06035-7102	0.46 ± 0.09	41.5 ± 4.1	26.8 ± 4.1	32.7 ± 4.1	37.2 ± 4.1	41.1 ± 4.0	11.8 ± 3.9	34.2 ± 3.9	23.9 ± 3.9	10.0 ± 3.9
IRAS 06206-6315	1.01 ± 0.20	16.8 ± 11.8	24.7 ± 5.3	29.5 ± 5.5	19.8 ± 5.3	19.3 ± 5.3	21.9 ± 4.6	21.6 ± 4.6	6.8 ± 5.2	—
IRAS 07598+6508	0.66 ± 0.01	28.5 ± 20.8	51.2 ± 12.1	15.7 ± 9.8	12.1 ± 8.4	—	37.4 ± 27.5	35.8 ± 22.8	42.2 ± 20.5	29.0 ± 23.6
IRAS 08311-2459	—	70.2 ± 6.7	76.9 ± 6.7	57.1 ± 6.9	53.8 ± 6.7	34.7 ± 6.7	50.5 ± 6.0	41.0 ± 6.2	52.6 ± 6.2	16.9 ± 6.2
IRAS 08572+3915	0.08 ± 0.01	6.6 ± 4.7	19.6 ± 7.7	—	6.2 ± 3.2	18.4 ± 2.5	10.9 ± 2.3	13.5 ± 2.3	5.6 ± 3.7	4.1 ± 3.1
IRAS 09022-3615	—	33.4 ± 2.3	41.4 ± 2.3	44.1 ± 2.4	39.7 ± 2.3	39.4 ± 2.3	28.5 ± 2.2	26.5 ± 2.2	19.9 ± 2.2	16.4 ± 2.2
IRAS 10378+1109	—	21.8 ± 13.5	57.0 ± 9.8	63.5 ± 9.8	54.7 ± 9.8	27.7 ± 9.8	39.0 ± 9.0	21.5 ± 9.0	11.0 ± 8.4	46.3 ± 9.0
IRAS 10565+2448	0.32 ± 0.03	13.3 ± 1.6	20.8 ± 1.6	16.0 ± 1.6	20.9 ± 1.6	15.2 ± 1.4	13.5 ± 1.4	10.9 ± 1.4	5.6 ± 1.4	5.4 ± 1.4
IRAS 11095-0238	0.38 ± 0.12	33.4 ± 6.2	10.9 ± 8.1	25.2 ± 6.2	35.6 ± 6.2	31.2 ± 6.3	37.0 ± 6.1	18.5 ± 6.1	21.2 ± 14.2	23.3 ± 6.1
IRAS 12071–0444	—	41.2 ± 8.6	50.5 ± 8.6	26.6 ± 8.7	43.0 ± 8.6	—	41.8 ± 8.0	23.1 ± 8.0	29.0 ± 8.0	—
IRAS 13120-5453	0.33 ± 0.02	25.8 ± 1.0	29.1 ± 1.0	30.5 ± 1.0	29.0 ± 1.0	21.8 ± 1.0	22.6 ± 1.0	14.8 ± 1.0	10.2 ± 1.0	8.0 ± 1.0
IRAS 13451+1232	0.47 ± 0.04	37.3 ± 9.1	16.4 ± 10.4	24.3 ± 9.0	13.0 ± 9.7	—	29.9 ± 8.3	19.0 ± 13.3	16.6 ± 12.4	11.2 ± 8.7
IRAS 14348-1447	0.83 ± 0.08	30.6 ± 4.8	31.3 ± 0.5	34.9 ± 5.0	49.6 ± 4.8	28.0 ± 4.9	41.3 ± 0.5	32.0 ± 0.5	14.7 ± 0.5	—
IRAS 14378-3651	0.26 ± 0.05	26.2 ± 3.4	18.8 ± 3.4	28.7 ± 3.5	19.7 ± 3.4	19.9 ± 3.2	16.3 ± 3.2	18.6 ± 3.2	14.9 ± 3.2	16.8 ± 3.2
IRAS 15250+3609	0.09 ± 0.03	7.9 ± 2.2	12.4 ± 2.2	13.4 ± 2.2	12.6 ± 2.2	8.9 ± 2.2	8.9 ± 2.2	9.4 ± 2.2	—	—
IRAS 15462-0450	0.16 ± 0.01	15.8 ± 5.3	10.9 ± 6.9	22.9 ± 5.4	13.7 ± 5.3	—	19.2 ± 4.9	7.1 ± 5.5	16.7 ± 4.9	17.1 ± 9.3
IRAS 16090-0139	0.67 ± 0.22	45.5 ± 1.1	36.2 ± 10.5	114.2 ± 110.4	120.3 ± 10.5	163.0 ± 10.5	110.0 ± 10.5	72.6 ± 10.4	52.4 ± 10.4	54.3 ± 10.4
IRAS 17208-0014	0.66 ± 0.07	25.3 ± 1.6	34.1 ± 1.6	35.5 ± 1.7	36.1 ± 1.6	31.2 ± 1.8	32.2 ± 1.9	17.8 ± 1.7	11.2 ± 1.7	9.8 ± 1.7
IRAS 19254-7245	0.51 ± 0.10	—	10.4 ± 2.5	18.5 ± 2.7	16.7 ± 2.5	19.1 ± 2.6	16.7 ± 2.4	11.4 ± 2.4	7.3 ± 2.4	12.1 ± 2.4
IRAS 19297-0406	0.51 ± 0.02	29.7 ± 5.4	27.3 ± 5.4	32.1 ± 5.7	43.9 ± 5.4	37.3 ± 5.5	13.2 ± 0.6	22.2 ± 0.6	8.4 ± 8.4	20.6 ± 5.5
IRAS 20087-0308	0.88 ± 0.03	65.5 ± 6.7	29.5 ± 6.7	56.0 ± 6.9	40.0 ± 6.7	27.6 ± 6.7	48.6 ± 6.6	31.2 ± 6.6	21.1 ± 12.7	30.6 ± 6.6
IRAS 20100-4156	0.48 ± 0.04	68.5 ± 11.1	19.3 ± 15.4	47.2 ± 11.6	65.1 ± 11.1	—	93.7 ± 11.4	37.2 ± 11.4	42.9 ± 25.9	28.7 ± 16.9
IRAS 20414-1651	0.17 ± 0.06	12.2 ± 8.7	7.2 ± 5.0	12.9 ± 4.8	19.4 ± 4.6	16.5 ± 4.6	19.1 ± 4.5	6.3 ± 4.2	22.9 ± 4.4	10.2 ± 5.8
IRAS 20551-4250	0.24 ± 0.05	17.5 ± 1.3	14.0 ± 1.3	20.0 ± 1.4	23.1 ± 1.3	16.5 ± 1.3	23.4 ± 1.3	21.3 ± 1.3	17.6 ± 1.3	15.6 ± 1.3
IRAS 22491-1808	0.27 ± 0.03	35.5 ± 3.4	22.1 ± 3.4	21.1 ± 4.4	31.9 ± 3.4	21.6 ± 3.5	39.6 ± 3.7	31.4 ± 3.8	29.1 ± 3.8	26.3 ± 3.8
IRAS 23128-5919	0.21 ± 0.04	12.7 ± 1.1	13.2 ± 1.1	19.1 ± 1.2	14.5 ± 1.1	14.3 ± 1.2	13.1 ± 1.2	10.6 ± 1.2	8.2 ± 1.2	11.0 ± 11.0
IRAS 23230-6926	—	25.6 ± 6.3	6.3 ± 6.3	30.1 ± 6.4	24.6 ± 6.3	35.7 ± 6.3	42.0 ± 5.9	23.9 ± 5.9	34.5 ± 5.9	27.6 ± 5.9
IRAS 23253-5415	—	17.4 ± 11.6	29.8 ± 8.5	30.5 ± 8.7	34.7 ± 8.5	43.3 ± 8.5	29.2 ± 23.2	17.3 ± 8.9	24.9 ± 8.9	23.9 ± 8.9
IRAS 23365+3604	0.37 ± 0.06	8.4 ± 2.9	22.1 ± 2.9	22.9 ± 3.0	14.5 ± 2.9	16.5 ± 2.9	26.4 ± 2.9	14.5 ± 2.9	17.6 ± 2.9	8.9 ± 2.9
UGC 5101	0.30 ± 0.03	11.0 ± 1.2	12.5 ± 1.2	9.0 ± 1.2	10.4 ± 1.2	7.7 ± 1.3	11.3 ± 1.3	7.8 ± 1.3	2.3 ± 1.3	5.0 ± 1.3
Mrk 231	0.35 ± 0.06	18.9 ± 1.3	18.8 ± 1.3	23.7 ± 1.4	28.0 ± 1.3	24.8 ± 1.3	28.8 ± 1.3	18.7 ± 1.3	16.8 ± 1.3	16.3 ± 1.3
Mrk 273	0.25 ± 0.03	12.7 ± 0.7	16.2 ± 0.7	17.0 ± 0.7	15.8 ± 0.7	13.1 ± 0.8	13.8 ± 0.8	7.6 ± 0.8	5.1 ± 0.8	5.5 ± 0.8
Mrk 463	0.11 ± 0.04	2.6 ± 2.4	5.7 ± 1.2	4.5 ± 1.3	3.9 ± 1.2	2.2 ± 1.9	2.3 ± 1.1	4.0 ± 3.7	3.3 ± 3.0	—
Arp 220	0.32 ± 0.03	15.3 ± 0.8	19.0 ± 0.8	19.8 ± 0.8	19.4 ± 0.8	18.0 ± 1.4	14.0 ± 1.5	11.0 ± 1.4	6.6 ± 1.4	4.4 ± 1.4
NGC 6240	0.43 ± 0.04	33.8 ± 1.0	38.2 ± 1.0	43.5 ± 1.0	43.2 ± 1.0	36.4 ± 1.0	33.6 ± 1.0	28.9 ± 1.0	22.7 ± 1.0	18.4 ± 1.0
Mrk 1014	0.35 ± 0.03	63.6 ± 14.3	87.1 ± 14.3	37.5 ± 14.5	—	—	22.2 ± 17.6	16.6 ± 10.3	—	30.4 ± 19.7

3.2. Component Luminosity Correlations

We next evaluate the Kendall-τ coefficients for each CO luminosity against L_{Sb}, L^{o}_{AGN}, L^{c}_{AGN}, and L_h (Figure 2). All of the CO luminosities correlate with L_{Sb}. For L_h, $L_{1–0}$ and $L_{5–4}$ through $L_{9–8}$ show correlations, though they may be weaker than those with L_{Sb}. However, $L_{10–9}$ and above do not show correlations with L_h. The starburst and host SFRs exhibit similar behavior to L_{Sb} and L_h. For L^{o}_{AGN} and L^{c}_{AGN} the $L_{10–9}$ and above luminosities show a correlation, but $L_{9–8}$ and below do not (see also, e.g., Esposito et al. [100]). The L^{o}_{AGN} and L^{c}_{AGN} luminosities show identical behaviour in these correlations, consistent with the inclination of the AGN obscurer relative to the line of sight not playing a dominant role in determining the observed CO line luminosities.

We next fit relations of the form in Equation (1) to those CO luminosities that show a correlation, for each of L_{Sb}, L^{o}_{AGN}, L_h, and $\dot{M}_{Sb}$. The results for L_{Sb} are:

$$\log(L_{1–0}) = 0.99 \pm 0.16 \log(L_{Sb}) - 6.35 \pm 1.92 \quad (12)$$
$$\log(L_{5–4}) = 0.99 \pm 0.16 \log(L_{Sb}) - 4.59 \pm 1.89 \quad (13)$$
$$\log(L_{6–5}) = 1.10 \pm 0.15 \log(L_{Sb}) - 5.85 \pm 1.79 \quad (14)$$
$$\log(L_{7–6}) = 0.98 \pm 0.12 \log(L_{Sb}) - 4.36 \pm 1.44 \quad (15)$$
$$\log(L_{8–7}) = 1.03 \pm 0.16 \log(L_{Sb}) - 4.99 \pm 1.88 \quad (16)$$
$$\log(L_{9–8}) = 1.16 \pm 0.22 \log(L_{Sb}) - 6.66 \pm 2.61 \quad (17)$$
$$\log(L_{10–9}) = 0.97 \pm 0.21 \log(L_{Sb}) - 4.36 \pm 2.50 \quad (18)$$
$$\log(L_{11–10}) = 0.65 \pm 0.18 \log(L_{Sb}) - 0.58 \pm 2.19 \quad (19)$$
$$\log(L_{12–11}) = 0.61 \pm 0.23 \log(L_{Sb}) - 0.09 \pm 2.80 \quad (20)$$
$$\log(L_{13–12}) = 0.14 \pm 0.16 \log(L_{Sb}) + 5.91 \pm 1.91 \quad (21)$$

The relations for $\dot{M}_{Sb}$ are:

$$\log(L_{1–0}) = 1.18 \pm 0.18 \log(\dot{M}_{Sb}) + 2.45 \pm 0.49 \quad (22)$$
$$\log(L_{5–4}) = 0.91 \pm 0.14 \log(\dot{M}_{Sb}) + 5.00 \pm 0.38 \quad (23)$$
$$\log(L_{6–5}) = 0.97 \pm 0.13 \log(\dot{M}_{Sb}) + 4.86 \pm 0.35 \quad (24)$$
$$\log(L_{7–6}) = 1.16 \pm 0.20 \log(\dot{M}_{Sb}) + 4.34 \pm 0.56 \quad (25)$$
$$\log(L_{8–7}) = 0.95 \pm 0.14 \log(\dot{M}_{Sb}) + 4.91 \pm 0.37 \quad (26)$$
$$\log(L_{9–8}) = 1.29 \pm 0.21 \log(\dot{M}_{Sb}) + 3.95 \pm 0.58 \quad (27)$$
$$\log(L_{10–9}) = 1.02 \pm 0.17 \log(\dot{M}_{Sb}) + 4.70 \pm 0.47 \quad (28)$$
$$\log(L_{11–10}) = 0.89 \pm 0.18 \log(\dot{M}_{Sb}) + 4.94 \pm 0.49 \quad (29)$$
$$\log(L_{12–11}) = 0.86 \pm 0.24 \log(\dot{M}_{Sb}) + 5.00 \pm 0.63 \quad (30)$$
$$\log(L_{13–12}) = 0.74 \pm 0.23 \log(\dot{M}_{Sb}) + 5.24 \pm 0.62 \quad (31)$$

For comparison, see, e.g., [101,102]. The results for L_h are:

$$\log(L_{1–0}) = 0.97 \pm 0.19 \log(L_h) - 5.11 \pm 2.13 \quad (32)$$
$$\log(L_{5–4}) = 1.03 \pm 0.20 \log(L_h) - 3.92 \pm 2.22 \quad (33)$$
$$\log(L_{6–5}) = 0.54 \pm 0.13 \log(L_h) + 1.40 \pm 1.45 \quad (34)$$
$$\log(L_{7–6}) = 0.97 \pm 0.24 \log(L_h) - 3.24 \pm 2.65 \quad (35)$$
$$\log(L_{8–7}) = 0.77 \pm 0.16 \log(L_h) - 0.94 \pm 1.73 \quad (36)$$
$$\log(L_{9–8}) = 1.00 \pm 0.27 \log(L_h) - 3.49 \pm 2.94 \quad (37)$$

The results for L^o_{AGN} are:

$$\log(L_{10\text{–}9}) = 0.78 \pm 0.17 \log(L^o_{AGN}) - 1.50 \pm 2.00 \quad (38)$$
$$\log(L_{11\text{–}10}) = 0.63 \pm 0.15 \log(L^o_{AGN}) + 0.06 \pm 1.76 \quad (39)$$
$$\log(L_{12\text{–}11}) = 0.77 \pm 0.19 \log(L^o_{AGN}) - 1.63 \pm 2.21 \quad (40)$$
$$\log(L_{13\text{–}12}) = 0.48 \pm 0.12 \log(L^o_{AGN}) + 1.70 \pm 1.44 \quad (41)$$

We plot some of these relations in Figure 3.

For $L_{1\text{–}0}$ and $L_{5\text{–}4}$ through $L_{9\text{–}8}$, the fits imply that the CO emission originates in the starburst and the host, with a smaller contribution from the AGN. Conversely, for $L_{10\text{–}9}$ and above, our results are consistent with the CO emission arising in the starburst and the AGN, with a smaller contribution from the host. In qualitative consistency with this result is that the $L_{Sb} - L_{CO}$ relations may tighten for objects optically classified as HII regions, and the $L_h - L_{CO}$ relations may tighten for systems with lower starburst lumnosities (Figures 3 and 4).

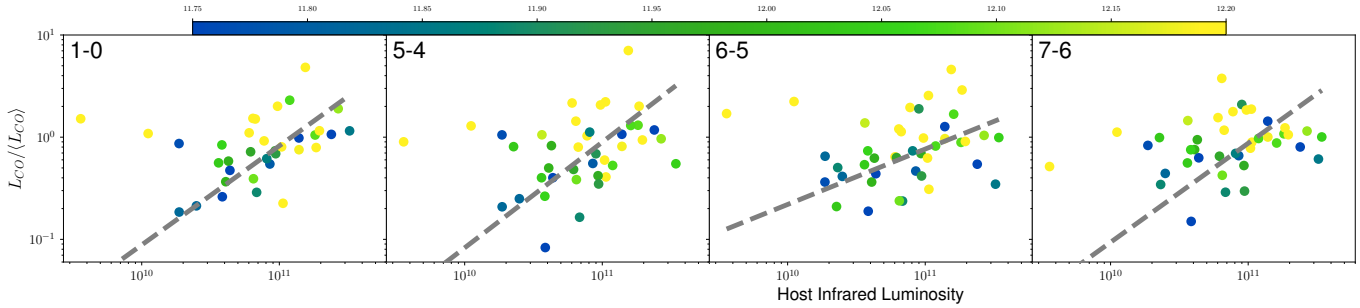

Figure 4. The $L_{CO} - L_h$ relations in Figure 3, color-coded by L_{Sb}. The relations may tighten for lower starburst luminosities, consistent with the CO gas being heated by both host and starburst starlight.

For L_{SB} and L_h, the slopes for the CO 9–8 and below relations are consistent with a linear relation. For CO 10–9 and above, the relations with L_{SB} are also consistent with linearity, though the slopes may start to flatten at CO 13–12. In contrast, the slopes for the relations between CO 10–9 and above, and L^o_{AGN}, are all consistent with being sub-linear.

We interpret these results as follows (see also, e.g., Greve et al. [65]). The CO 9–8 and below lines primarily arise from radiative heating in the starburst and the host, with a smaller contribution from the AGN. In the higher J transitions, host heating becomes insignificant. The emission in these CO lines primarily arises from starburst and AGN activity. In addition, mechanical heating and shocks become important for producing CO 11-10 and above.

3.3. Multi-Component Fits

To facilitate comparisons with galaxy evolution models, we present two-component fits of the form $L_{CO} = \alpha L_A + \beta L_B + \gamma$, where the luminosities L_A and L_B are chosen based on the results of the Kendall-τ tests; starburst and host of CO 9–8 and below, and starburst and AGN for CO 10–9 and above. This yields:

$$L_{1-0} = (3.82 \pm 0.70)\frac{L_{Sb}}{10^7} + (4.93 \pm 1.58)\frac{L_h}{10^6} - (3.47 \pm 1.44) \times 10^5 \quad (42)$$

$$L_{5-4} = (1.36 \pm 0.32)\frac{L_{Sb}}{10^5} + (1.57 \pm 0.40)\frac{L_h}{10^4} - (5.96 \pm 3.90) \times 10^6 \quad (43)$$

$$L_{6-5} = (1.42 \pm 0.29)\frac{L_{Sb}}{10^5} + (8.57 \pm 2.02)\frac{L_h}{10^5} - (1.28 \pm 3.21) \times 10^6 \quad (44)$$

$$L_{7-6} = (1.15 \pm 0.50)\frac{L_{Sb}}{10^5} + (5.30 \pm 1.79)\frac{L_h}{10^4} - (9.41 \pm 9.39) \times 10^6 \quad (45)$$

$$L_{8-7} = (1.29 \pm 0.33)\frac{L_{Sb}}{10^5} + (1.78 \pm 0.41)\frac{L_h}{10^4} - (3.58 \pm 3.86) \times 10^6 \quad (46)$$

$$L_{9-8} = (1.24 \pm 0.48)\frac{L_{Sb}}{10^5} + (1.27 \pm 0.50)\frac{L_h}{10^4} - (2.10 \pm 5.24) \times 10^6 \quad (47)$$

$$L_{10-9} = (1.16 \pm 0.51)\frac{L_{Sb}}{10^5} + (9.91 \pm 2.69)\frac{L^o_{AGN}}{10^5} - (7.20 \pm 7.61) \times 10^6 \quad (48)$$

$$L_{11-10} = (2.53 \pm 3.71)\frac{L_{Sb}}{10^6} + (6.08 \pm 1.53)\frac{L^o_{AGN}}{10^5} + (3.16 \pm 5.08) \times 10^6 \quad (49)$$

$$L_{12-11} = (2.37 \pm 3.79)\frac{L_{Sb}}{10^6} + (7.66 \pm 1.91)\frac{L^o_{AGN}}{10^5} - (3.00 \pm 5.51) \times 10^6 \quad (50)$$

$$L_{13-12} = (-2.53 \pm 2.46)\frac{L_{Sb}}{10^6} + (2.12 \pm 0.70)\frac{L^o_{AGN}}{10^5} + (9.03 \pm 3.06) \times 10^6 \quad (51)$$

These fits are consistent with the log–linear fits, though they suggest the AGN may be the dominant contributor to the CO 11–10 and above emission. The fits are given in Figure 5. We do not present fits of the form: $L_{CO} = \alpha L_{Sb} + \beta L_{AGN} + \gamma L_h$ as they proved challenging to constrain with the number of objects in our sample.

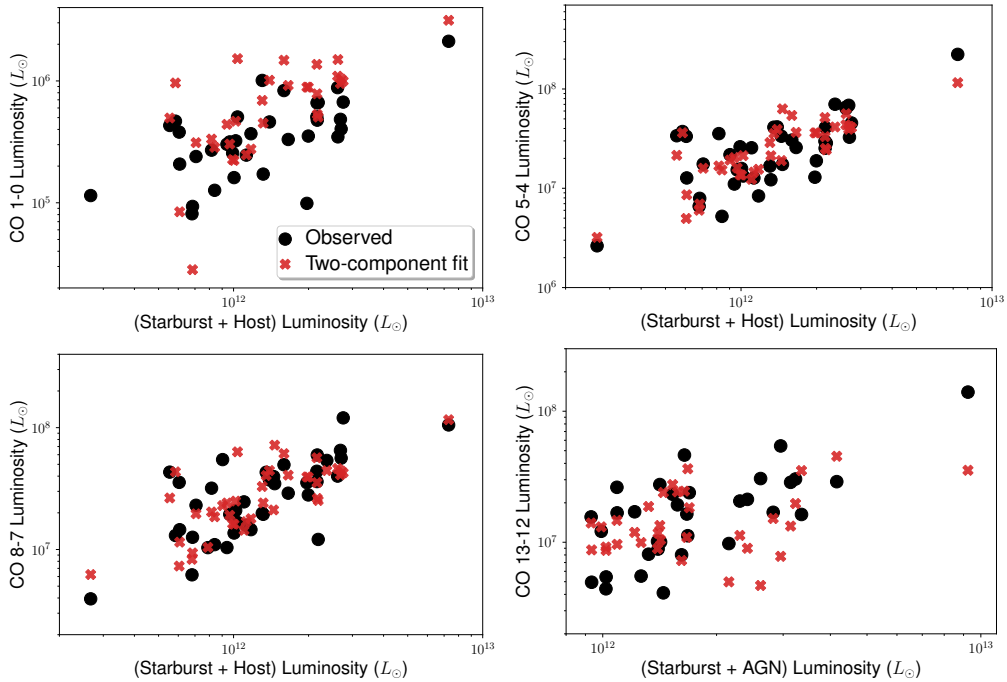

Figure 5. Example comparisons between CO luminosity and the sum of two component luminosities (starburst and host for 1–0, 5–4, and 8–7, starburst and AGN for 13–12). The red crosses show the results for a linear fit between the two component luminosities and the CO luminosity, of the form $L_{CO} = \alpha L_A + \beta L_B + \gamma$ (Section 3.3).

3.4. Star Formation Rate—Molecular Gas Scaling Relations

As an alternative diagnostic of the relation between the cold ISM and star formation (see, e.g., [103,104] for reviews) in our sample, we consider the relation between SFR and

cold molecular hydrogen mass. To do so, we use the cold H_2 masses for our sample as summarized in Farrah et al. [2]. Since the total SFR is dominated in most cases by the starburst, we first fit a relation of the form in Equation (1). We obtain:

$$\log(M_{H_2}) = 1.11 \pm 0.19 \log(\dot{M}_{Sb}) + 6.92 \pm 0.49 \quad (52)$$

This is consistent with the proposed universal scaling relation of Lada et al. [105]. Instead using a two-component model yields:

$$M_{H_2} = (2.01 \pm 0.34) \times 10^7 \dot{M}_{Sb} + (5.84 \pm 1.95) \times 10^8 \dot{M}_h - (3.05 \pm 1.53) \times 10^8 \quad (53)$$

We note though that Equation (53) does not give substantially reduced scatter relative to Equation (52). These results are summarized in Figure 6.

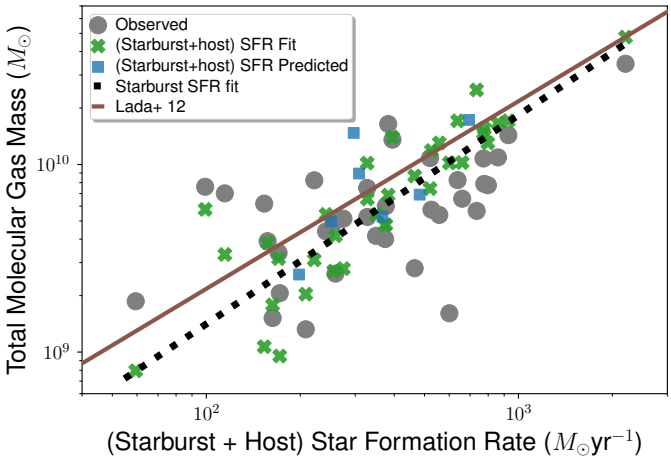

Figure 6. The relation between total SFR and total molecular gas mass (Section 3.4). Overplotted are our starburst SFR—M_{H_2} fit (Equation (52)), our starburst + host SFR—M_{H_2} fit (Equation (53)), and the predicted positions of objects without a CO 1–0 luminosity from Equation (53). Also plotted is the SFR-M_{H_2} scaling relation from Lada et al. [105].

3.5. Starburst Efficiency

We next examine whether or not AGN luminosity can affect the heating of CO by the starburst. To do so, we consider the L_{Sb}/L_{CO} ratio as a function of L^c_{AGN}, via the relation

$$\log\left(\frac{L_{Sb}}{L_{CO}}\right) = \alpha \log L^c_{AGN} + \beta \quad (54)$$

For the whole sample, we find a mildly negative relation between L_{Sb}/L_{CO} and L^c_{AGN} in most CO lines (Figure 7). Combined with the results from Section 3.1, this can be interpreted as a significant contribution to heating the CO by the AGN in the CO 9–8 and above lines. We do not find that the AGN affects the starburst heating of the molecular gas, at least for the sample as a whole (see also, e.g., Shangguan et al. [106], Zhuang et al. [107], Valentino et al. [108] but also McKinney et al. [109]). We note though that the factors that affect fueling of star formation in infrared-luminous mergers are subtle, and may vary by location within individual sources (e.g., [110]).

Evidence for a relation between L_{Sb}/L_{CO} and L^c_{AGN} emerges when dividing the sample into two sub-samples at $\tau_V \sim 170$ and fitting relations of the form in Equation (54). The $\tau_V > 170$ sub-sample yields the same or slightly more negative slopes than the full sample—that is, similar trends in CO luminosity per unit starburst luminosity, as AGN luminosity increases. Conversely, the $\tau_V < 170$ sub-sample shows marginally positive slopes, suggesting less CO luminosity per unit starburst luminosity, as AGN luminosity increases. However, though the formal uncertainties imply this difference is highly sig-

nificant, simulations that divide the sample in two equal sub-samples at random give an estimated confidence of 3σ.

To interpret this result, we assume that the direct AGN contribution to producing CO emission is insignificant in all lines below CO 10–9, and sub-dominant for CO 10–9 and above. We also assume that the CO emission is not significantly absorbed. Our result is then consistent with more luminous AGN reducing the ability of star formation to produce warm and hot CO in starbursts with *lower* initial optical depths (see also, e.g., Song et al. [111]). This effect can be interpreted as negative AGN feedback [89,112–118], though the effect is subtle, and unlikely to be a viable channel to globally quench star formation in infrared-luminous galaxies. We speculate that the origin of the effect is that higher optical depth starbursts have higher ISM densities, which are harder to disrupt by a luminous AGN (see also, e.g., [119,120]).

Other explanations seem less plausible. We do not see a dependence on the depth of the 9.8 µm silicate feature, or on the ratio of polycyclic aromatic hydrocarbon equivalent widths, suggesting that this effect does not arise in compact obscured nuclei [121]. More extincted starbursts could just be less luminous, but we see no such trend between L_{Sb} and τ_V. Alternatively, more extincted starbursts could be intrinsically more efficient at heating molecular gas. If this were true though, then no trends with AGN luminosity would be expected.

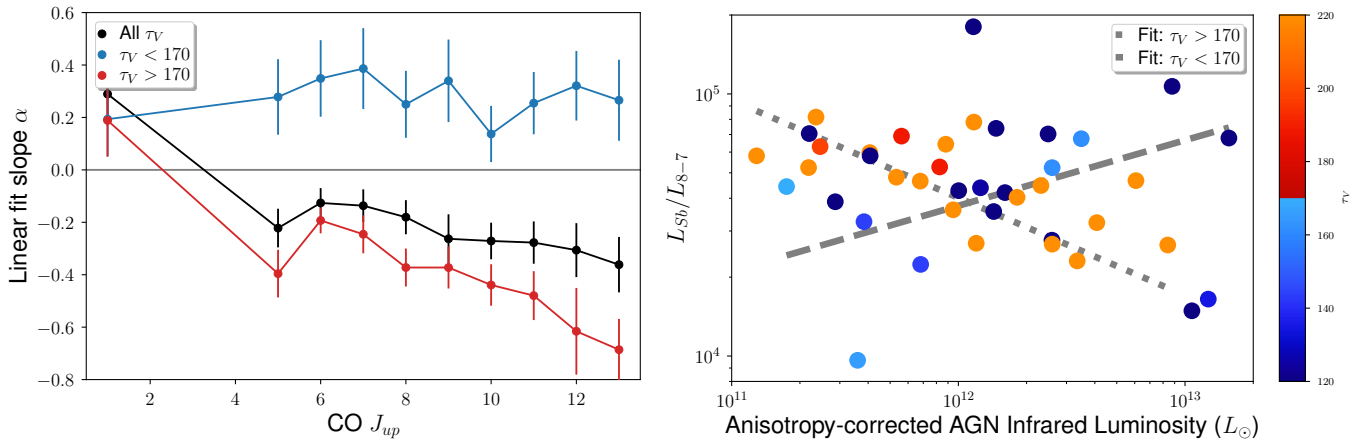

Figure 7. (**Left**) The slopes of the L_{Sb}/L_{CO} vs. L^c_{AGN} relations from Equation (54) (Section 3.5), plotted as a function of CO transition. The slopes are shown for the whole sample, and for the $\tau_V > 170$ and $\tau_V < 170$ sub-samples. (**Right**) An example of the L_{Sb}/L_{CO} vs. L^c_{AGN} relation, for L_{8-7}. Also shown are the individual fits for the $\tau_V > 170$ and $\tau_V < 170$ subsamples.

4. Conclusions

We have studied the origin of CO emission in a sample of 42 infrared-luminous galaxy mergers at $z < 0.27$ with infrared luminosities in excess of 10^{12} $L_\odot$. To do so, we take results from a recent radiative transfer modelling study of this sample, which decomposes their infrared luminosities into contributions from star formation, AGN activity, and the host galaxy. We then compare these component luminosities to archival measures of the integrated CO luminosities in the 1–0, and 5–4 through 13–12 transitions. Our conclusions are:

1. The luminosities of the CO 1–0 and 5–4 through 13–12 lines are consistent with an origin in one or both of ongoing star formation, and heating by starlight in the host galaxy. We do not find evidence for a significant contribution to these lines from AGN activity.
2. We present log–linear relations between the CO luminosities in the 1–0 and 5–4 through 13–12 transitions, and with the starburst and host galaxy luminosities. The slopes of these relations suggest an origin of the CO emission in gas heating.
3. The luminosities of the CO 10–9 through 13–12 lines are consistent with an origin in one or both of the starburst and the AGN. We do not find evidence for a significant

contribution from the host galaxy. The slopes of the relations between these CO line luminosities and the starburst and AGN luminosities may be sub-linear, which is consistent with a contribution to these lines from mechanical heating and shocks.

4. We also present two-component linear model fits between each CO line luminosity and infrared component luminosities. For CO 9–8 and below we fit against starburst and host luminosity. For CO 10–9 and above we fit against starburst and AGN luminosity. These fits are consistent with the log–linear model fits, and give straightforward conversions that can be used in galaxy simulations.
5. For the sample as a whole, we find no evidence for a relation between AGN luminosity and the L_{CO}/L_{Sb}, in any CO line. This suggests that a more luminous AGN does not reduce the efficiency by which the starburst heats the molecular gas. There is, however, evidence for a dependence on starburst initial optical depth (τ_V). Starbursts with low τ_V may heat the CO 5–4 transitions and above less efficiently. This is consistent with mild negative AGN feedback.

Author Contributions: Conceptualization, D.F. and A.E.; methodology, D.F.; software, A.E.; validation, D.F., A.E. and S.P.; formal analysis, D.F.; investigation, D.F.; resources, D.F., A.E., J.A., D.L.C., K.C., E.H., M.J., V.L., A.L., C.L., C.P., S.P., L.K.P., D.R., A.V. and L.W.; data curation, D.F.; writing—original draft preparation, D.F. and A.E.; writing—review and editing, J.A., D.L.C., K.C., E.H., M.J., V.L., A.L., C.L., C.P., S.P., L.K.P., D.R., A.V. and L.W.; visualization, D.F., A.E., A.L. and S.P.; supervision, D.F.; project administration, D.F. and A.E.; All authors have read and agreed to the published version of the manuscript.

Funding: This research received no external funding.

Data Availability Statement: All the data used in this paper are publicly available within this paper, or within the references cited.

Acknowledgments: J.A. acknowledges support from the Science and Technology Foundation (FCT, Portugal) through research grants PTDC/FIS-AST/29245/2017, UIDB/04434/2020 and UIDP/04434/2020. For the purpose of open access, the author(s) has applied a Creative Commons Attribution (CC BY) licence to any Author Accepted Manuscript version arising.

Conflicts of Interest: The authors declare no conflict of interest.

Note

[1] In contrast, 'warm' H_2 can be observed directly in the near- and mid-infrared [15,55], but comprises only a small fraction of the total molecular gas mass.

References

1. Rowan-Robinson, M.; Wang, L.; Farrah, D.; Rigopoulou, D.; Gruppioni, C.; Vaccari, M.; Marchetti, L.; Clements, D.L.; Pearson, W.J. Extreme submillimetre starburst galaxies. *Astron. Astrophys.* **2018**, *619*, A169. [CrossRef]
2. Farrah, D.; Efstathiou, A.; Afonso, J.; Bernard-Salas, J.; Cairns, J.; Clements, D.L.; Croker, K.; Hatziminaoglou, E.; Joyce, M.; Lacy, M.; et al. Stellar and black hole assembly in z < 0.3 infrared-luminous mergers: Intermittent starbursts versus super-Eddington accretion. *Mon. Not. R. Astron. Soc.* **2022**, *513*, 4770–4786. [CrossRef]
3. Murphy, T.W., Jr.; Armus, L.; Matthews, K.; Soifer, B.T.; Mazzarella, J.M.; Shupe, D.L.; Strauss, M.A.; Neugebauer, G. Visual and Near-Infrared Imaging of Ultraluminous Infrared Galaxies: The IRAS 2 Jy Sample. *Astron. J.* **1996**, *111*, 1025. [CrossRef]
4. Genzel, R.; Tacconi, L.J.; Rigopoulou, D.; Lutz, D.; Tecza, M. Ultraluminous Infrared Mergers: Elliptical Galaxies in Formation? *Astrophys. J.* **2001**, *563*, 527–545. [CrossRef]
5. Farrah, D.; Rowan-Robinson, M.; Oliver, S.; Serjeant, S.; Borne, K.; Lawrence, A.; Lucas, R.A.; Bushouse, H.; Colina, L. HST/WFPC2 imaging of the QDOT ultraluminous infrared galaxy sample. *Mon. Not. R. Astron. Soc.* **2001**, *326*, 1333–1352. [CrossRef]
6. Bushouse, H.A.; Borne, K.D.; Colina, L.; Lucas, R.A.; Rowan-Robinson, M.; Baker, A.C.; Clements, D.L.; Lawrence, A.; Oliver, S. Ultraluminous Infrared Galaxies: Atlas of Near-Infrared Images. *Astrophys. J. Suppl.* **2002**, *138*, 1–18. [CrossRef]
7. Haan, S.; Surace, J.A.; Armus, L.; Evans, A.S.; Howell, J.H.; Mazzarella, J.M.; Kim, D.C.; Vavilkin, T.; Inami, H.; Sanders, D.B.; et al. The Nuclear Structure in Nearby Luminous Infrared Galaxies: Hubble Space Telescope NICMOS Imaging of the GOALS Sample. *Astron. J.* **2011**, *141*, 100. [CrossRef]

8. Kim, D.C.; Evans, A.S.; Vavilkin, T.; Armus, L.; Mazzarella, J.M.; Sheth, K.; Surace, J.A.; Haan, S.; Howell, J.H.; Díaz-Santos, T.; et al. Hubble Space Telescope ACS Imaging of the GOALS Sample: Quantitative Structural Properties of Nearby Luminous Infrared Galaxies with $L_{IR} > 10^{11.4}$ $L_{\odot}$. *Astrophys. J.* **2013**, *768*, 102. [CrossRef]
9. Petty, S.M.; Armus, L.; Charmandaris, V.; Evans, A.S.; Le Floc'h, E.; Bridge, C.; Díaz-Santos, T.; Howell, J.H.; Inami, H.; Psychogyios, A.; et al. The FUV to Near-IR Morphologies of Luminous Infrared Galaxies in the Goals Sample. *Astron. J.* **2014**, *148*, 111. [CrossRef]
10. Genzel, R.; Lutz, D.; Sturm, E.; Egami, E.; Kunze, D.; Moorwood, A.F.M.; Rigopoulou, D.; Spoon, H.W.W.; Sternberg, A.; Tacconi-Garman, L.E.; et al. What Powers Ultraluminous IRAS Galaxies? *Astrophys. J.* **1998**, *498*, 579–605. [CrossRef]
11. Farrah, D.; Afonso, J.; Efstathiou, A.; Rowan-Robinson, M.; Fox, M.; Clements, D. Starburst and AGN activity in ultraluminous infrared galaxies. *Mon. Not. R. Astron. Soc.* **2003**, *343*, 585–607. [CrossRef]
12. Farrah, D.; Surace, J.A.; Veilleux, S.; Sanders, D.B.; Vacca, W.D. Space Telescope Imaging Spectrograph Ultraviolet/Optical Spectroscopy of "Warm" Ultraluminous Infrared Galaxies. *Astrophys. J.* **2005**, *626*, 70–88. [CrossRef]
13. Armus, L.; Charmandaris, V.; Bernard-Salas, J.; Spoon, H.W.W.; Marshall, J.A.; Higdon, S.J.U.; Desai, V.; Teplitz, H.I.; Hao, L.; Devost, D.; et al. Observations of Ultraluminous Infrared Galaxies with the Infrared Spectrograph on the Spitzer Space Telescope. II. The IRAS Bright Galaxy Sample. *Astrophys. J.* **2007**, *656*, 148–167. [CrossRef]
14. Nardini, E.; Risaliti, G.; Salvati, M.; Sani, E.; Watabe, Y.; Marconi, A.; Maiolino, R. Exploring the active galactic nucleus and starburst content of local ultraluminous infrared galaxies through 5-8 μm spectroscopy. *Mon. Not. R. Astron. Soc.* **2009**, *399*, 1373–1402. [CrossRef]
15. Bernard-Salas, J.; Spoon, H.W.W.; Charmandaris, V.; Lebouteiller, V.; Farrah, D.; Devost, D.; Brandl, B.R.; Wu, Y.; Armus, L.; Hao, L.; et al. A Spitzer High-resolution Mid-Infrared Spectral Atlas of Starburst Galaxies. *Astrophys. J. Suppl.* **2009**, *184*, 230–247. [CrossRef]
16. Farrah, D.; Lebouteiller, V.; Spoon, H.W.W.; Bernard-Salas, J.; Pearson, C.; Rigopoulou, D.; Smith, H.A.; González-Alfonso, E.; Clements, D.L.; Efstathiou, A.; et al. Far-infrared Fine-structure Line Diagnostics of Ultraluminous Infrared Galaxies. *Astrophys. J.* **2013**, *776*, 38. [CrossRef]
17. Farrah, D.; Baloković, M.; Stern, D.; Harris, K.; Kunimoto, M.; Walton, D.J.; Alexander, D.M.; Arévalo, P.; Ballantyne, D.R.; Bauer, F.E.; et al. The Geometry of the Infrared and X-ray Obscurer in a Dusty Hyperluminous Quasar. *Astrophys. J.* **2016**, *831*, 76. [CrossRef]
18. Pereira-Santaella, M.; Colina, L.; García-Burillo, S.; Lamperti, I.; González-Alfonso, E.; Perna, M.; Arribas, S.; Alonso-Herrero, A.; Aalto, S.; Combes, F.; et al. Physics of ULIRGs with MUSE and ALMA: The PUMA project. II. Are local ULIRGs powered by AGN? The subkiloparsec view of the 220 GHz continuum. *Astron. Astrophys.* **2021**, *651*, A42. [CrossRef]
19. Tacconi, L.J.; Genzel, R.; Lutz, D.; Rigopoulou, D.; Baker, A.J.; Iserlohe, C.; Tecza, M. Ultraluminous Infrared Galaxies: QSOs in Formation? *Astrophys. J.* **2002**, *580*, 73–87. [CrossRef]
20. Farrah, D.; Lacy, M.; Priddey, R.; Borys, C.; Afonso, J. Evidence that FeLoBALs May Signify the Transition between an Ultraluminous Infrared Galaxy and a Quasar. *Astrophys. J. Lett.* **2007**, *662*, L59–L62. [CrossRef]
21. Farrah, D.; Connolly, B.; Connolly, N.; Spoon, H.W.W.; Oliver, S.; Prosper, H.B.; Armus, L.; Houck, J.R.; Liddle, A.R.; Desai, V. An Evolutionary Paradigm for Dusty Active Galaxies at Low Redshift. *Astrophys. J.* **2009**, *700*, 395–416. [CrossRef]
22. Farrah, D.; Verma, A.; Oliver, S.; Rowan-Robinson, M.; McMahon, R. Hubble Space Telescope Wide Field Planetary Camera 2 observations of hyperluminous infrared galaxies. *Mon. Not. R. Astron. Soc.* **2002**, *329*, 605–619. [CrossRef]
23. Kartaltepe, J.S.; Dickinson, M.; Alexander, D.M.; Bell, E.F.; Dahlen, T.; Elbaz, D.; Faber, S.M.; Lotz, J.; McIntosh, D.H.; Wiklind, T.; et al. GOODS-Herschel and CANDELS: The Morphologies of Ultraluminous Infrared Galaxies at $z \sim 2$. *Astrophys. J.* **2012**, *757*, 23. [CrossRef]
24. Farrah, D.; Petty, S.; Connolly, B.; Blain, A.; Efstathiou, A.; Lacy, M.; Stern, D.; Lake, S.; Jarrett, T.; Bridge, C.; et al. The Role of the Most Luminous Obscured AGNs in Galaxy Assembly at $z \sim 2$. *Astrophys. J.* **2017**, *844*, 106. [CrossRef]
25. Zavala, J.A.; Aretxaga, I.; Dunlop, J.S.; Michałowski, M.J.; Hughes, D.H.; Bourne, N.; Chapin, E.; Cowley, W.; Farrah, D.; Lacey, C.; et al. The SCUBA-2 Cosmology Legacy Survey: The EGS deep field—II. Morphological transformation and multiwavelength properties of faint submillimetre galaxies. *Mon. Not. R. Astron. Soc.* **2018**, *475*, 5585–5602. [CrossRef]
26. Gullberg, B.; Smail, I.; Swinbank, A.M.; Dudzevičiūtė, U.; Stach, S.M.; Thomson, A.P.; Almaini, O.; Chen, C.C.; Conselice, C.; Cooke, E.A.; et al. An ALMA survey of the SCUBA-2 Cosmology Legacy Survey UKIDSS/UDS field: High-resolution dust continuum morphologies and the link between sub-millimetre galaxies and spheroid formation. *Mon. Not. R. Astron. Soc.* **2019**, *490*, 4956–4974. [CrossRef]
27. Farrah, D.; Serjeant, S.; Efstathiou, A.; Rowan-Robinson, M.; Verma, A. Submillimetre observations of hyperluminous infrared galaxies. *Mon. Not. R. Astron. Soc.* **2002**, *335*, 1163–1175. [CrossRef]
28. Alexander, D.M.; Bauer, F.E.; Chapman, S.C.; Smail, I.; Blain, A.W.; Brandt, W.N.; Ivison, R.J. The X-ray Spectral Properties of SCUBA Galaxies. *Astrophys. J.* **2005**, *632*, 736–750. [CrossRef]
29. Hatziminaoglou, E.; Pérez-Fournon, I.; Polletta, M.; Afonso-Luis, A.; Hernán-Caballero, A.; Montenegro-Montes, F.M.; Lonsdale, C.; Xu, C.K.; Franceschini, A.; Rowan-Robinson, M.; et al. Sloan Digital Sky Survey Quasars in the Spitzer Wide-Area Infrared Extragalactic Survey (SWIRE) ELAIS N1 Field: Properties and Spectral Energy Distributions. *Astron. J.* **2005**, *129*, 1198–1211. [CrossRef]

30. Heinis, S.; Buat, V.; Béthermin, M.; Aussel, H.; Bock, J.; Boselli, A.; Burgarella, D.; Conley, A.; Cooray, A.; Farrah, D.; et al. HERMES: Unveiling obscured star formation—The far-infrared luminosity function of ultraviolet-selected galaxies at z ∼ 1.5. *Mon. Not. R. Astron. Soc.* **2013**, *429*, 1113–1132. [CrossRef]
31. Bussmann, R.S.; Riechers, D.; Fialkov, A.; Scudder, J.; Hayward, C.C.; Cowley, W.I.; Bock, J.; Calanog, J.; Chapman, S.C.; Cooray, A.; et al. HerMES: ALMA Imaging of Herschel-selected Dusty Star-forming Galaxies. *Astrophys. J.* **2015**, *812*, 43. [CrossRef]
32. Harris, K.; Farrah, D.; Schulz, B.; Hatziminaoglou, E.; Viero, M.; Anderson, N.; Béthermin, M.; Chapman, S.; Clements, D.L.; Cooray, A.; et al. Star formation rates in luminous quasars at 2 < z < 3. *Mon. Not. R. Astron. Soc.* **2016**, *457*, 4179–4194. [CrossRef]
33. Pitchford, L.K.; Hatziminaoglou, E.; Feltre, A.; Farrah, D.; Clarke, C.; Harris, K.A.; Hurley, P.; Oliver, S.; Page, M.; Wang, L. Extreme star formation events in quasar hosts over 0.5 < z < 4. *Mon. Not. R. Astron. Soc.* **2016**, *462*, 4067–4077. [CrossRef]
34. Simpson, J.M.; Smail, I.; Swinbank, A.M.; Ivison, R.J.; Dunlop, J.S.; Geach, J.E.; Almaini, O.; Arumugam, V.; Bremer, M.N.; Chen, C.C.; et al. The SCUBA-2 Cosmology Legacy Survey: Multi-wavelength Properties of ALMA-identified Submillimeter Galaxies in UKIDSS UDS. *Astrophys. J.* **2017**, *839*, 58. [CrossRef]
35. Bourne, N.; Dunlop, J.S.; Merlin, E.; Parsa, S.; Schreiber, C.; Castellano, M.; Conselice, C.J.; Coppin, K.E.K.; Farrah, D.; Fontana, A.; et al. Evolution of cosmic star formation in the SCUBA-2 Cosmology Legacy Survey. *Mon. Not. R. Astron. Soc.* **2017**, *467*, 1360–1385. [CrossRef]
36. Marrone, D.P.; Spilker, J.S.; Hayward, C.C.; Vieira, J.D.; Aravena, M.; Ashby, M.L.N.; Bayliss, M.B.; Béthermin, M.; Brodwin, M.; Bothwell, M.S.; et al. Galaxy growth in a massive halo in the first billion years of cosmic history. *Nature* **2018**, *553*, 51–54. [CrossRef] [PubMed]
37. Stach, S.M.; Smail, I.; Swinbank, A.M.; Simpson, J.M.; Geach, J.E.; An, F.X.; Almaini, O.; Arumugam, V.; Blain, A.W.; Chapman, S.C.; et al. An ALMA Survey of the SCUBA-2 Cosmology Legacy Survey UKIDSS/UDS Field: Number Counts of Submillimeter Galaxies. *Astrophys. J.* **2018**, *860*, 161. [CrossRef]
38. Małek, K.; Buat, V.; Roehlly, Y.; Burgarella, D.; Hurley, P.D.; Shirley, R.; Duncan, K.; Efstathiou, A.; Papadopoulos, A.; Vaccari, M.; et al. HELP: Modelling the spectral energy distributions of Herschel detected galaxies in the ELAIS N1 field. *Astron. Astrophys.* **2018**, *620*, A50. [CrossRef]
39. Pitchford, L.K.; Farrah, D.; Alatalo, K.; Afonso, J.; Efstathiou, A.; Hatziminaoglou, E.; Lacy, M.; Urrutia, T.; Violino, G. The mid-infrared and CO gas properties of an extreme star-forming FeLoBAL quasar. *Mon. Not. R. Astron. Soc.* **2019**, *487*, 3130–3139. [CrossRef]
40. Wang, L.; Gao, F.; Best, P.N.; Duncan, K.; Hardcastle, M.J.; Kondapally, R.; Małek, K.; McCheyne, I.; Sabater, J.; Shimwell, T.; et al. The bright end of the infrared luminosity functions and the abundance of hyperluminous infrared galaxies. *Astron. Astrophys.* **2021**, *648*, A8. [CrossRef]
41. Gao, F.; Wang, L.; Efstathiou, A.; Małek, K.; Best, P.N.; Bonato, M.; Farrah, D.; Kondapally, R.; McCheyne, I.; Röttgering, H.J.A. The nature of hyperluminous infrared galaxies. *Astron. Astrophys.* **2021**, *654*, A117. [CrossRef]
42. Efstathiou, A.; Małek, K.; Burgarella, D.; Hurley, P.; Oliver, S.; Buat, V.; Shirley, R.; Duivenvoorden, S.; Lesta, V.P.; Farrah, D.; et al. A hyperluminous obscured quasar at a redshift of $z = 4.3$. *Mon. Not. R. Astron. Soc.* **2021**, *503*, L11–L16. [CrossRef]
43. Sanders, D.B.; Mirabel, I.F. Luminous Infrared Galaxies. *Annu. Rev. Astron. Astrophys.* **1996**, *34*, 749. [CrossRef]
44. Blain, A.W.; Smail, I.; Ivison, R.J.; Kneib, J.P.; Frayer, D.T. Submillimeter galaxies. *Phys. Rep.* **2002**, *369*, 111–176. [CrossRef]
45. Lonsdale, C.J.; Farrah, D.; Smith, H.E. Ultraluminous Infrared Galaxies. In *Astrophysics Update 2*; Mason, J.W., Ed.; Springer: Berlin/Heidelberg, Germany, 2006; p. 285. [CrossRef]
46. Casey, C.M.; Narayanan, D.; Cooray, A. Dusty star-forming galaxies at high redshift. *Phys. Rep.* **2014**, *541*, 45–161. [CrossRef]
47. Farrah, D.; Smith, K.E.; Ardila, D.; Bradford, C.M.; Dipirro, M.; Ferkinhoff, C.; Glenn, J.; Goldsmith, P.; Leisawitz, D.; Nikola, T.; et al. Review: Far-infrared instrumentation and technological development for the next decade. *J. Astron. Telesc. Instrum. Syst.* **2019**, *5*, 020901. [CrossRef]
48. Pérez-Torres, M.; Mattila, S.; Alonso-Herrero, A.; Aalto, S.; Efstathiou, A. Star formation and nuclear activity in luminous infrared galaxies: An infrared through radio review. *Astron. Astrophys. Rev.* **2021**, *29*, 2. [CrossRef]
49. Sajina, A.; Lacy, M.; Pope, A. The Past and Future of Mid-Infrared Studies of AGN. *Universe* **2022**, *8*, 356. [CrossRef]
50. Solomon, P.M.; Vanden Bout, P.A. Molecular Gas at High Redshift. *Annu. Rev. Astron. Astrophys.* **2005**, *43*, 677–725. [CrossRef]
51. Cicone, C.; Maiolino, R.; Sturm, E.; Graciá-Carpio, J.; Feruglio, C.; Neri, R.; Aalto, S.; Davies, R.; Fiore, F.; Fischer, J.; et al. Massive molecular outflows and evidence for AGN feedback from CO observations. *Astron. Astrophys.* **2014**, *562*, A21. [CrossRef]
52. George, R.D.; Ivison, R.J.; Smail, I.; Swinbank, A.M.; Hopwood, R.; Stanley, F.; Swinyard, B.M.; Valtchanov, I.; Werf, P.P.v.d. Herschel reveals a molecular outflow in a z = 2.3 ULIRG. *Mon. Not. R. Astron. Soc.* **2014**, *442*, 1877–1883. [CrossRef]
53. Tombesi, F.; Meléndez, M.; Veilleux, S.; Reeves, J.N.; González-Alfonso, E.; Reynolds, C.S. Wind from the black-hole accretion disk driving a molecular outflow in an active galaxy. *Nature* **2015**, *519*, 436–438. [CrossRef] [PubMed]
54. Ishibashi, W.; Fabian, A.C. What powers galactic outflows: Nuclear starbursts or AGN? *Mon. Not. R. Astron. Soc.* **2022**, *516*, 4963–4970. [CrossRef]
55. Higdon, S.J.U.; Armus, L.; Higdon, J.L.; Soifer, B.T.; Spoon, H.W.W. A Spitzer Space Telescope Infrared Spectrograph Survey of Warm Molecular Hydrogen in Ultraluminous Infrared Galaxies. *Astrophys. J.* **2006**, *648*, 323–339. [CrossRef]
56. Solomon, P.M.; Downes, D.; Radford, S.J.E.; Barrett, J.W. The Molecular Interstellar Medium in Ultraluminous Infrared Galaxies. *Astrophys. J.* **1997**, *478*, 144–161. [CrossRef]

57. Greve, T.R.; Bertoldi, F.; Smail, I.; Neri, R.; Chapman, S.C.; Blain, A.W.; Ivison, R.J.; Genzel, R.; Omont, A.; Cox, P.; et al. An interferometric CO survey of luminous submillimetre galaxies. *Mon. Not. R. Astron. Soc.* **2005**, *359*, 1165–1183. [CrossRef]
58. Carilli, C.L.; Walter, F. Cool Gas in High-Redshift Galaxies. *Annu. Rev. Astron. Astrophys.* **2013**, *51*, 105–161. [CrossRef]
59. Bolatto, A.D.; Wolfire, M.; Leroy, A.K. The CO-to-H_2 Conversion Factor. *Annu. Rev. Astron. Astrophys.* **2013**, *51*, 207–268. [CrossRef]
60. Genzel, R.; Tacconi, L.J.; Lutz, D.; Saintonge, A.; Berta, S.; Magnelli, B.; Combes, F.; García-Burillo, S.; Neri, R.; Bolatto, A.; et al. Combined CO and Dust Scaling Relations of Depletion Time and Molecular Gas Fractions with Cosmic Time, Specific Star-formation Rate, and Stellar Mass. *Astrophys. J.* **2015**, *800*, 20. [CrossRef]
61. Saintonge, A.; Catinella, B.; Tacconi, L.J.; Kauffmann, G.; Genzel, R.; Cortese, L.; Davé, R.; Fletcher, T.J.; Graciá-Carpio, J.; Kramer, C.; et al. xCOLD GASS: The Complete IRAM 30 m Legacy Survey of Molecular Gas for Galaxy Evolution Studies. *Astrophys. J. Suppl.* **2017**, *233*, 22. [CrossRef]
62. Yamashita, T.; Komugi, S.; Matsuhara, H.; Armus, L.; Inami, H.; Ueda, J.; Iono, D.; Kohno, K.; Evans, A.S.; Arimatsu, K. Cold Molecular Gas Along the Merger Sequence in Local Luminous Infrared Galaxies. *Astrophys. J.* **2017**, *844*, 96. [CrossRef]
63. Molina, J.; Ibar, E.; Villanueva, V.; Escala, A.; Cheng, C.; Baes, M.; Messias, H.; Yang, C.; Bauer, F.E.; van der Werf, P.; et al. VALES V: a kinematic analysis of the molecular gas content in H-ATLAS galaxies at z $\sim$ 0.03-0.35 using ALMA. *Mon. Not. R. Astron. Soc.* **2019**, *482*, 1499–1524. [CrossRef]
64. Weiß, A.; Downes, D.; Neri, R.; Walter, F.; Henkel, C.; Wilner, D.J.; Wagg, J.; Wiklind, T. Highly-excited CO emission in APM 08279+5255 at z = 3.9. *Astron. Astrophys.* **2007**, *467*, 955–969. [CrossRef]
65. Greve, T.R.; Leonidaki, I.; Xilouris, E.M.; Weiß, A.; Zhang, Z.Y.; van der Werf, P.; Aalto, S.; Armus, L.; Díaz-Santos, T.; Evans, A.S.; et al. Star Formation Relations and CO Spectral Line Energy Distributions across the J-ladder and Redshift. *Astrophys. J.* **2014**, *794*, 142. [CrossRef]
66. Rosenberg, M.J.F.; van der Werf, P.P.; Aalto, S.; Armus, L.; Charmandaris, V.; Díaz-Santos, T.; Evans, A.S.; Fischer, J.; Gao, Y.; González-Alfonso, E.; et al. The Herschel Comprehensive (U)LIRG Emission Survey (HERCULES): CO Ladders, Fine Structure Lines, and Neutral Gas Cooling. *Astrophys. J.* **2015**, *801*, 72. [CrossRef]
67. Mashian, N.; Sturm, E.; Sternberg, A.; Janssen, A.; Hailey-Dunsheath, S.; Fischer, J.; Contursi, A.; González-Alfonso, E.; Graciá-Carpio, J.; Poglitsch, A.; et al. High-J CO Sleds in Nearby Infrared Bright Galaxies Observed By Herschel/PACS. *Astrophys. J.* **2015**, *802*, 81. [CrossRef]
68. Pearson, C.; Rigopoulou, D.; Hurley, P.; Farrah, D.; Afonso, J.; Bernard-Salas, J.; Borys, C.; Clements, D.L.; Cormier, D.; Efstathiou, A.; et al. HERUS: A CO Atlas from SPIRE Spectroscopy of Local ULIRGs. *Astrophys. J. Suppl.* **2016**, *227*, 9. [CrossRef]
69. Scott, K.S.; Lupu, R.E.; Aguirre, J.E.; Auld, R.; Aussel, H.; Baker, A.J.; Beelen, A.; Bock, J.; Bradford, C.M.; Brisbin, D.; et al. Redshift Determination and CO Line Excitation Modeling for the Multiply Lensed Galaxy HLSW-01. *Astrophys. J.* **2011**, *733*, 29. [CrossRef]
70. Aravena, M.; Carilli, C.L.; Salvato, M.; Tanaka, M.; Lentati, L.; Schinnerer, E.; Walter, F.; Riechers, D.; Smolcić, V.; Capak, P.; et al. Deep observations of CO line emission from star-forming galaxies in a cluster candidate at z = 1.5. *Mon. Not. R. Astron. Soc.* **2012**, *426*, 258–275. [CrossRef]
71. van der Tak, F.F.S.; Black, J.H.; Schöier, F.L.; Jansen, D.J.; van Dishoeck, E.F. A computer program for fast non-LTE analysis of interstellar line spectra. With diagnostic plots to interpret observed line intensity ratios. *Astron. Astrophys.* **2007**, *468*, 627–635. [CrossRef]
72. Kamenetzky, J.; Privon, G.C.; Narayanan, D. Recovering the Physical Properties of Molecular Gas in Galaxies from CO SLED Modeling. *Astrophys. J.* **2018**, *859*, 9. [CrossRef]
73. Efstathiou, A.; Farrah, D.; Afonso, J.; Clements, D.L.; González-Alfonso, E.; Lacy, M.; Oliver, S.; Papadopoulou Lesta, V.; Pearson, C.; Rigopoulou, D.; et al. A new look at local ultraluminous infrared galaxies: The atlas and radiative transfer models of their complex physics. *Mon. Not. R. Astron. Soc.* **2022**, *512*, 5183–5213. [CrossRef]
74. Spoon, H.W.W.; Farrah, D.; Lebouteiller, V.; González-Alfonso, E.; Bernard-Salas, J.; Urrutia, T.; Rigopoulou, D.; Westmoquette, M.S.; Smith, H.A.; Afonso, J.; et al. Diagnostics of AGN-Driven Molecular Outflows in ULIRGs from Herschel-PACS Observations of OH at 119 µm. *Astrophys. J.* **2013**, *775*, 127. [CrossRef]
75. Clements, D.L.; Pearson, C.; Farrah, D.; Greenslade, J.; Bernard-Salas, J.; González-Alfonso, E.; Afonso, J.; Efstathiou, A.; Rigopoulou, D.; Lebouteiller, V.; et al. HERUS: the far-IR/submm spectral energy distributions of local ULIRGs and photometric atlas. *Mon. Not. R. Astron. Soc.* **2018**, *475*, 2097–2121. [CrossRef]
76. Kamenetzky, J.; Rangwala, N.; Glenn, J.; Maloney, P.R.; Conley, A. L_{CO}/L_{FIR} Relations with CO Rotational Ladders of Galaxies Across the Herschel SPIRE Archive. *Astrophys. J.* **2016**, *829*, 93. [CrossRef]
77. Sanders, D.B.; Scoville, N.Z.; Zensus, A.; Soifer, B.T.; Wilson, T.L.; Zylka, R.; Steppe, H. Detection of CO (1–>0) emission from infrared quasars and luminous Seyfert galaxies. *Astron. Astrophys.* **1989**, *213*, L5–L8.
78. Mirabel, I.F.; Booth, R.S.; Garay, G.; Johansson, L.E.B.; Sanders, D.B. CO(1–0) emission from luminous infrared galaxies in the southern hemisphere. *Astron. Astrophys.* **1990**, *236*, 327–332.
79. Downes, D.; Solomon, P.M.; Radford, S.J.E. Molecular Gas Mass and Far-Infrared Emission from Distant Luminous Galaxies. *Astrophys. J. Lett.* **1993**, *414*, L13. [CrossRef]
80. Baan, W.A.; Henkel, C.; Loenen, A.F.; Baudry, A.; Wiklind, T. Dense gas in luminous infrared galaxies. *Astron. Astrophys.* **2008**, *477*, 747–762. [CrossRef]

81. Chung, A.; Narayanan, G.; Yun, M.S.; Heyer, M.; Erickson, N.R. The Redshift Search Receiver Observations of ^{12}CO J = 1 → 0 in 29 Ultraluminous Infrared Galaxies. *Astron. J.* **2009**, *138*, 858–872. [CrossRef]
82. Greve, T.R.; Papadopoulos, P.P.; Gao, Y.; Radford, S.J.E. Molecular Gas in Extreme Star-Forming Environments: The Starbursts Arp 220 and NGC 6240 as Case Studies. *Astrophys. J.* **2009**, *692*, 1432–1446. [CrossRef]
83. Braun, R.; Popping, A.; Brooks, K.; Combes, F. Molecular gas in intermediate-redshift ultraluminous infrared galaxies. *Mon. Not. R. Astron. Soc.* **2011**, *416*, 2600–2606. [CrossRef]
84. Papadopoulos, P.P.; van der Werf, P.P.; Xilouris, E.M.; Isaak, K.G.; Gao, Y.; Mühle, S. The molecular gas in luminous infrared galaxies—I. CO lines, extreme physical conditions and their drivers. *Mon. Not. R. Astron. Soc.* **2012**, *426*, 2601–2629. [CrossRef]
85. Xia, X.Y.; Gao, Y.; Hao, C.N.; Tan, Q.H.; Mao, S.; Omont, A.; Flaquer, B.O.; Leon, S.; Cox, P. Molecular Gas in Infrared Ultraluminous QSO Hosts. *Astrophys. J.* **2012**, *750*, 92. [CrossRef]
86. Meijerink, R.; Kristensen, L.E.; Weiß, A.; van der Werf, P.P.; Walter, F.; Spaans, M.; Loenen, A.F.; Fischer, J.; Israel, F.P.; Isaak, K.; et al. Evidence for CO Shock Excitation in NGC 6240 from Herschel SPIRE Spectroscopy. *Astrophys. J. Lett.* **2013**, *762*, L16. [CrossRef]
87. Ueda, J.; Iono, D.; Yun, M.S.; Crocker, A.F.; Narayanan, D.; Komugi, S.; Espada, D.; Hatsukade, B.; Kaneko, H.; Matsuda, Y.; et al. Cold Molecular Gas in Merger Remnants. I. Formation of Molecular Gas Disks. *Astrophys. J. Suppl.* **2014**, *214*, 1. [CrossRef]
88. Sliwa, K.; Wilson, C.D.; Aalto, S.; Privon, G.C. Extreme CO Isotopic Abundances in the ULIRG IRAS 13120-5453: An Extremely Young Starburst or Top-heavy Initial Mass Function. *Astrophys. J. Lett.* **2017**, *840*, L11. [CrossRef]
89. Gowardhan, A.; Spoon, H.; Riechers, D.A.; González-Alfonso, E.; Farrah, D.; Fischer, J.; Darling, J.; Fergulio, C.; Afonso, J.; Bizzocchi, L. The Dual Role of Starbursts and Active Galactic Nuclei in Driving Extreme Molecular Outflows. *Astrophys. J.* **2018**, *859*, 35. [CrossRef]
90. Ruffa, I.; Vignali, C.; Mignano, A.; Paladino, R.; Iwasawa, K. The role of molecular gas in the nuclear regions of IRAS 00183-7111. ALMA and X-ray investigations of an ultraluminous infrared galaxy. *Astron. Astrophys.* **2018**, *616*, A127. [CrossRef]
91. Brown, T.; Wilson, C.D. Extreme CO Isotopologue Line Ratios in ULIRGS: Evidence for a Top-heavy IMF. *Astrophys. J.* **2019**, *879*, 17. [CrossRef]
92. Herrero-Illana, R.; Privon, G.C.; Evans, A.S.; Díaz-Santos, T.; Pérez-Torres, M.Á.; U, V.; Alberdi, A.; Iwasawa, K.; Armus, L.; Aalto, S.; et al. Molecular gas and dust properties of galaxies from the Great Observatories All-sky LIRG Survey. *Astron. Astrophys.* **2019**, *628*, A71. [CrossRef]
93. Fotopoulou, C.M.; Dasyra, K.M.; Combes, F.; Salomé, P.; Papachristou, M. Complex molecular gas kinematics in the inner 5 kpc of 4C12.50 as seen by ALMA. *Astron. Astrophys.* **2019**, *629*, A30. [CrossRef]
94. Tan, Q.H.; Gao, Y.; Daddi, E.; Xia, X.Y.; Hao, C.N.; Omont, A.; Kohno, K. Deep Observations of CO and Free-Free Emission in Ultraluminous Infrared QSO IRAS F07599+6508. *Astrophys. J.* **2021**, *913*, 82. [CrossRef]
95. Efstathiou, A.; Siebenmorgen, R. Starburst and cirrus models for submillimeter galaxies. *Astron. Astrophys.* **2009**, *502*, 541–548. [CrossRef]
96. Efstathiou, A.; Rowan-Robinson, M. Dusty discs in active galactic nuclei. *Mon. Not. R. Astron. Soc.* **1995**, *273*, 649–661. [CrossRef]
97. Efstathiou, A.; Hough, J.H.; Young, S. A model for the infrared continuum spectrum of NGC 1068. *Mon. Not. R. Astron. Soc.* **1995**, *277*, 1134–1144. [CrossRef]
98. Efstathiou, A.; Christopher, N.; Verma, A.; Siebenmorgen, R. Active galactic nucleus torus models and the puzzling infrared spectrum of IRAS F10214+4724. *Mon. Not. R. Astron. Soc.* **2013**, *436*, 1873–1882. [CrossRef]
99. Boggs, P.T.; Byrd, R.H.; Schnabel, R.B. A stable and efficient algorithm for nonlinear orthogonal distance regression. *SIAM J. Sci. Stat. Comput.* **1987**, *8*, 1052–1078. [CrossRef]
100. Esposito, F.; Vallini, L.; Pozzi, F.; Casasola, V.; Mingozzi, M.; Vignali, C.; Gruppioni, C.; Salvestrini, F. AGN impact on the molecular gas in galactic centres as probed by CO lines. *Mon. Not. R. Astron. Soc.* **2022**, *512*, 686–711. [CrossRef]
101. Hunt, L.K.; Tortora, C.; Ginolfi, M.; Schneider, R. Scaling relations and baryonic cycling in local star-forming galaxies. II. Gas content and star-formation efficiency. *Astron. Astrophys.* **2020**, *643*, A180. [CrossRef]
102. Sánchez-García, M.; Pereira-Santaella, M.; García-Burillo, S.; Colina, L.; Alonso-Herrero, A.; Villar-Martín, M.; Saito, T.; Díaz-Santos, T.; Piqueras López, J.; Arribas, S.; et al. Duality in spatially resolved star formation relations in local LIRGs. *Astron. Astrophys.* **2022**, *659*, A102. [CrossRef]
103. Tacconi, L.J.; Genzel, R.; Sternberg, A. The Evolution of the Star-Forming Interstellar Medium Across Cosmic Time. *Annu. Rev. Astron. Astrophys.* **2020**, *58*, 157–203. [CrossRef]
104. Saintonge, A.; Catinella, B. The Cold Interstellar Medium of Galaxies in the Local Universe. *Annu. Rev. Astron. Astrophys.* **2022**, *60*, 319–361. [CrossRef]
105. Lada, C.J.; Forbrich, J.; Lombardi, M.; Alves, J.F. Star Formation Rates in Molecular Clouds and the Nature of the Extragalactic Scaling Relations. *Astrophys. J.* **2012**, *745*, 190. [CrossRef]
106. Shangguan, J.; Ho, L.C.; Bauer, F.E.; Wang, R.; Treister, E. AGN Feedback and Star Formation of Quasar Host Galaxies: Insights from the Molecular Gas. *Astrophys. J.* **2020**, *899*, 112. [CrossRef]
107. Zhuang, M.Y.; Ho, L.C.; Shangguan, J. Black Hole Accretion Correlates with Star Formation Rate and Star Formation Efficiency in Nearby Luminous Type 1 Active Galaxies. *Astrophys. J.* **2021**, *906*, 38. [CrossRef]

108. Valentino, F.; Daddi, E.; Puglisi, A.; Magdis, G.E.; Kokorev, V.; Liu, D.; Madden, S.C.; Gómez-Guijarro, C.; Lee, M.Y.; Cortzen, I.; et al. The effect of active galactic nuclei on the cold interstellar medium in distant star-forming galaxies. *Astron. Astrophys.* **2021**, *654*, A165. [CrossRef]
109. McKinney, J.; Armus, L.; Pope, A.; Díaz-Santos, T.; Charmandaris, V.; Inami, H.; Song, Y.; Evans, A.S. Regulating Star Formation in Nearby Dusty Galaxies: Low Photoelectric Efficiencies in the Most Compact Systems. *Astrophys. J.* **2021**, *908*, 238. [CrossRef]
110. Thorp, M.D.; Ellison, S.L.; Pan, H.A.; Lin, L.; Patton, D.R.; Bluck, A.F.L.; Walters, D.; Scudder, J.M. The ALMaQUEST Survey X: What powers merger induced star formation? *Mon. Not. R. Astron. Soc.* **2022**, *516*, 1462–1480. [CrossRef]
111. Song, Y.; Linden, S.T.; Evans, A.S.; Barcos-Muñoz, L.; Privon, G.C.; Yoon, I.; Murphy, E.J.; Larson, K.L.; Díaz-Santos, T.; Armus, L.; et al. A Comparison between Nuclear Ring Star Formation in LIRGs and in Normal Galaxies with the Very Large Array. *Astrophys. J.* **2021**, *916*, 73. [CrossRef]
112. Westmoquette, M.S.; Clements, D.L.; Bendo, G.J.; Khan, S.A. Spatially resolved observations of warm ionized gas and feedback in local ULIRGs. *Mon. Not. R. Astron. Soc.* **2012**, *424*, 416–456. [CrossRef]
113. Fabian, A.C. Observational Evidence of Active Galactic Nuclei Feedback. *Annu. Rev. Astron. Astrophys.* **2012**, *50*, 455–489. [CrossRef]
114. Farrah, D.; Urrutia, T.; Lacy, M.; Efstathiou, A.; Afonso, J.; Coppin, K.; Hall, P.B.; Lonsdale, C.; Jarrett, T.; Bridge, C.; et al. Direct Evidence for Termination of Obscured Star Formation by Radiatively Driven Outflows in Reddened QSOs. *Astrophys. J.* **2012**, *745*, 178. [CrossRef]
115. Bridge, C.R.; Blain, A.; Borys, C.J.K.; Petty, S.; Benford, D.; Eisenhardt, P.; Farrah, D.; Griffith, R.L.; Jarrett, T.; Lonsdale, C.; et al. A New Population of High-z, Dusty Lyα Emitters and Blobs Discovered by WISE: Feedback Caught in the Act? *Astrophys. J.* **2013**, *769*, 91. [CrossRef]
116. Baron, D.; Netzer, H.; Poznanski, D.; Prochaska, J.X.; Förster Schreiber, N.M. Evidence of ongoing AGN-driven feedback in a quiescent post-starburst E+A galaxy. *Mon. Not. R. Astron. Soc.* **2017**, *470*, 1687–1702. [CrossRef]
117. González-Alfonso, E.; Fischer, J.; Spoon, H.W.W.; Stewart, K.P.; Ashby, M.L.N.; Veilleux, S.; Smith, H.A.; Sturm, E.; Farrah, D.; Falstad, N.; et al. Molecular Outflows in Local ULIRGs: Energetics from Multitransition OH Analysis. *Astrophys. J.* **2017**, *836*, 11. [CrossRef]
118. Longinotti, A.L.; Vega, O.; Krongold, Y.; Aretxaga, I.; Yun, M.; Chavushyan, V.; Feruglio, C.; Gómez-Ruiz, A.; Montaña, A.; León-Tavares, J.; et al. Early Science with the Large Millimeter Telescope: An Energy-driven Wind Revealed by Massive Molecular and Fast X-ray Outflows in the Seyfert Galaxy IRAS 17020+4544. *Astrophys. J. Lett.* **2018**, *867*, L11. [CrossRef]
119. Mukherjee, D.; Wagner, A.Y.; Bicknell, G.V.; Morganti, R.; Oosterloo, T.; Nesvadba, N.; Sutherland, R.S. The jet-ISM interactions in IC 5063. *Mon. Not. R. Astron. Soc.* **2018**, *476*, 80–95. [CrossRef]
120. Mackey, J.; Walch, S.; Seifried, D.; Glover, S.C.O.; Wünsch, R.; Aharonian, F. Non-equilibrium chemistry and destruction of CO by X-ray flares. *Mon. Not. R. Astron. Soc.* **2019**, *486*, 1094–1122. [CrossRef]
121. García-Bernete, I.; Rigopoulou, D.; Aalto, S.; Spoon, H.W.W.; Hernán-Caballero, A.; Efstathiou, A.; Roche, P.F.; König, S. A technique to select the most obscured galaxy nuclei. *Astron. Astrophys.* **2022**, *663*, A46. [CrossRef]